

# Broad distribution of crystal field environments for Nd<sup>3+</sup> in Calcite

S. H. Withers, R. E. Peale\*, A. Schulte, G. Braunstein,  
*University of Central Florida, Department of Physics, Orlando, FL 32816*

K. M. Beck and W. P. Hess  
*William R. Wiley Environmental Molecular Sciences Laboratory, Pacific Northwest National Laboratory,  
Richland, WA*

R. J. Reeder  
*Department of Geosciences, State University of New York, Stony Brook, NY 11794-2100*

\*Corresponding author: email [rep@physics.ucf.edu](mailto:rep@physics.ucf.edu), phone (407)823-3076, fax (407)823-5112

## Abstract

Calcite micro-crystals were grown from solution with single crystal dimensions up to 3 mm and doped up to ~0.1 atomic % with Nd<sup>3+</sup> ions. Phase purity was verified by powder x-ray diffraction. The concentration of Nd<sup>3+</sup> was measured by energy-dispersive spectrometry and Rutherford backscattering spectrometry. Micro x-ray fluorescence mapping of the calcite grains indicates uniform Nd distribution in as-grown crystal grains. X-ray absorption fine structure suggests that Nd<sup>3+</sup> is substituted for Ca<sup>2+</sup> with local lattice distortion. Temperature dependent near-infrared spectroscopy of Nd<sup>3+</sup> impurities in calcite reveals large inhomogeneous linewidths and smooth line profiles that are characteristic of glassy hosts, though the samples are well crystallized.

Keywords: Calcium carbonate; Calcite; Neodymium; Carbonate minerals; Nuclear waste

## Introduction

Calcite ( $\text{CaCO}_3$ ) is one of the most reactive mineral components in Earth's near-surface environment. It plays an important role in impurity sorption processes in soil and groundwater systems (Mecherri et al. 1990). The common occurrence of calcium carbonate at localities impacted by radionuclide waste has focused attention on the effectiveness of calcite in the sequestration of actinides. For example, carbonate minerals are present at the Hanford Nuclear Reservation in Eastern Washington State as grain coatings, particles, and as thick subsurface caliche layers (Slate 1996). Understanding of uptake processes, including adsorption and coprecipitation, and characterization of contaminants in carbonates are important for remediation efforts.

Calcite readily takes up divalent metal impurity ions in the  $\text{Ca}^{2+}$  position (Reeder et al. 1999), which is 6-fold coordinated to  $\text{O}^{2-}$  ions. Uptake has been reported for ions much larger (e.g.,  $\text{Pb}^{2+}$  and  $\text{Ba}^{2+}$ ) and smaller (e.g.,  $\text{Co}^{2+}$  and  $\text{Zn}^{2+}$ ) than  $\text{Ca}^{2+}$  causing only local lattice distortions (Reeder et al. 2000). Less is known about heterovalent substitutions in calcite. Trivalent rare earth elements (REEs) are strongly partitioned into calcite (Zhong and Mucci 1995), which suggests that calcite may play a strong role in determining their environmental fate. The uptake behavior of lanthanides is of particular interest because their chemical behavior is similar to that of the trivalent actinides (e.g.,  $\text{Pu}^{3+}$ ,  $\text{Am}^{3+}$ ,  $\text{Cm}^{3+}$ ). The latter group poses serious challenges for environmental remediation, yet, owing to their toxicity or radioactivity, can be problematic for laboratory study.

This paper focuses on  $\text{Nd}^{3+}$  coprecipitated with calcite. Nd is usually considered the most important of the REEs from the environmental perspective because it is closest to  $\text{Am}^{3+}$  and  $\text{Cm}^{3+}$  in size. The ionic radius of  $\text{Nd}^{3+}$  (0.983 Å) is comparable to that of  $\text{Ca}^{2+}$  (1.00 Å) with six-fold coordination (Shannon 1976). The Ca site in calcite forms a nearly regular octahedron with all six Ca-O distances equal to 2.36 Å (Effenberger et al. 1981).  $\text{Nd}^{3+}$  is expected to occupy the  $\text{Ca}^{2+}$  site, as trivalent lanthanides are known to show a strong preference for substitution in Ca sites (Bünzli and Choppin 1989). X-ray absorption fine structure (XAFS) studies of the Lanthanide series in synthetic calcite show that the local oxygen coordination changes from 6-fold to 7-fold as the ionic radius increases (Elzinga et al. in press), and the largest ion studied,  $\text{Nd}^{3+}$ , is 7-fold, which requires disruption of the local lattice structure. Possible mechanisms to account for the extra oxygen ligation have been suggested, including bidentate linkage of one carbonate group, or retention of an  $\text{OH}^-$  or  $\text{H}_2\text{O}$  from the REE hydration shell (Elzinga et al. in press). Since increased coordination is only observed for larger trivalent REEs, it is unlikely that it can be attributed solely to the requirement of charge compensation. Hence, there remain fundamental scientific questions regarding  $\text{Nd}^{3+}$  in calcite.

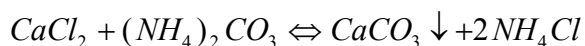
Substitution of trivalent impurity ions for divalent host ions requires charge compensation since the host crystal must remain electrically neutral. Charge compensation is intimately related to the local structure surrounding the impurity, and it may involve local lattice distortion, defects, or other impurities. High-resolution low temperature optical spectroscopy of  $\text{Nd}^{3+}$  heterovalently substituted for divalent ions in apatite crystals has revealed that the required charge compensation can occur in a wide variety of ways (Peale et al. 1995). The effect of charge compensation is revealed by

shifts in optical transition frequencies (absorption and luminescence lines) caused by changes in the local crystal field environment. Because defects and impurities occupy discrete lattice positions, an ensemble of densely grouped distinct lines, which can be isolated by site selective photoluminescence, characterizes the spectra of these crystals. Occasionally, a smooth, generally weak background is also seen (Peale et al. 1995). The relative strength of the different contributions can depend strongly on REE concentration (Peale et al. 1995).

The optical spectrum of  $\text{Nd}^{3+}$  in calcite has not been reported. In this paper,  $\text{Nd}^{3+}$  is introduced into calcite crystals by solution growth in order to learn about local site structure from optical spectroscopy. A considerable part of this paper is aimed at verifying the structure and doping of the solution grown crystals.

## Experiment

$\text{CaCO}_3$  crystals were grown from a room-temperature solution of 2 % by mass  $\text{CaCl}_2$  and 21 % by mass  $\text{NH}_4\text{Cl}$ . Solid  $(\text{NH}_4)_2\text{CO}_3$  was suspended above the solution in the headspace of the sealed reaction vessel.  $\text{CaCO}_3$  forms after vapor diffusion of  $\text{CO}_2$  and  $\text{NH}_3$  into solution per the overall equation



as described by Gruzensky (1967). The near steady-state breakdown of  $(\text{NH}_4)_2\text{CO}_3$  allows growth of large calcite crystals, up to 3 mm in this case.  $\text{Nd}^{3+}$  doped crystals were grown by the same method with 0.065 % by mass  $\text{NdCl}_3 \cdot 6\text{H}_2\text{O}$  added to the growth solution. Crystals were filtered from the growth solution after 30 days, thoroughly rinsed

with deionized water, and dried in air. The as-grown crystal morphology was observed under a 45 X stereo microscope.

The composition of the samples was characterized by Rutherford backscattering spectrometry (RBS) and by energy-dispersive spectrometry (EDS). RBS was performed using a 2.25 MeV alpha particle beam on Nd:CaCO<sub>3</sub> pressed pellet samples. Data reduction was performed using the program RUMP (Doolittle 1985). EDS spectra were measured by scanning a focused electron beam over an area on the surface of a single powder granule.

Powder x-ray diffraction (Cu K<sub>α</sub> radiation) was used to determine the crystal phase of the samples by comparison with database spectra using JADE (1995). Samples were ground in acetone with a mortar and pestle until relative diffraction peak intensities were repeatable after sample rearrangement.

Micro X-ray fluorescence (μXRF) mapping was performed at the Advanced Photon Source (APS), PNC-CAT, beam line 20-ID at Argonne National Lab. Nd doped calcite grains were mounted on high purity silica glass slides and polished flat. The incident x-ray beam was focused to a 5 x 5 μm<sup>2</sup> spot that was rastered over the sample surface, which was positioned for 30° angle of incidence. Resultant Nd-L<sub>α</sub> and Ca-K<sub>α</sub> fluorescence were measured with a 13-element Ge detector positioned at 90° with respect to the incident X-ray beam.

XAFS experiments were performed at beamlines 20-ID and 20-BM at the APS on the grown Nd:CaCO<sub>3</sub> and standard Neodymium carbonate (Acros) Nd<sub>2</sub>(CO<sub>3</sub>)<sub>3</sub>·xH<sub>2</sub>O respectively. Nd<sup>3+</sup> doped calcite samples were ground into fine powder and spread evenly onto clear tape. Nine layers were used to produce the desired edge step. Four

layers of  $\text{Nd}_2(\text{CO}_3)_3 \cdot x\text{H}_2\text{O}$  powder on kapton tape were used. Si(111) monochromator crystals were used to produce a monochromatic beam, with one crystal detuned 25% to reduce harmonics. Nd  $L_3$ -edge (6.208 keV) fluorescence yield from Nd: $\text{CaCO}_3$  was measured with a 13-element Ge detector.  $\text{Nd}_2(\text{CO}_3)_3 \cdot x\text{H}_2\text{O}$   $L_3$ -edge spectra were measured using transmission methods. XAFS fits were performed using the program WinXAS (Ressler 1997) using theoretical phases and amplitudes calculated using the program FEFF6 (Rehr et al. 1992). The starting model for FEFF6 calculations assumed that Nd substituted in the Ca site of calcite.

Pressed pellets were made for most of the optical experiments discussed in this paper. Doped or undoped  $\text{CaCO}_3$  was mixed with 10% by volume KBr and ground into fine powder. The powder was pressed into translucent disks at 10,000 psi to a thickness of 0.5 mm. Pressed pellets were made for control spectra by mixing 0.1 weight %  $\text{NdCl}_3 \cdot 6\text{H}_2\text{O}$  or 1 weight %  $\text{Nd}_2(\text{CO}_3)_3 \cdot x\text{H}_2\text{O}$  with KBr.

Transmission spectroscopy was performed at the University of Central Florida using a Bomem DA8 Fourier spectrometer. Near-IR and visible transmittance measurements used a quartz-halogen lamp, quartz beam splitter, and a Si detector. Cooled InSb and HgCdTe detectors were used for transmittance measurements into the mid-IR. Mid-IR spectra were collected on synthetic calcite single crystals with ~mm dimensions and compared with spectra for plates of natural calcite. The sample thickness (mid-IR beam path) in each case was 300  $\mu\text{m}$ . Low temperature spectra were obtained using a CTI-Cryogenics closed-cycle cooler with sample temperature monitored by a Si diode mounted on the copper cold finger. Samples were thermally contacted to the cold finger with rubber cement.

Near IR fluorescence spectroscopy was collected using a micro-spectroscopy setup with 488 nm excitation from an Argon ion laser (~3mW). As-grown samples were mounted on the x-y-z translation stage of a microscope and sampled with a long working distance 40 X objective. The fluorescence was analyzed with a single-grating spectrograph (Instruments SA, HR 640) equipped with a CCD detector (Princeton Instruments). Low temperature spectra were obtained using a small liquid-nitrogen cold finger cryostat. The wavelength scale was calibrated against five sharp  $^4F_{3/2} \rightarrow ^4I_{9/2}$  luminescence lines from 2% Nd:SVAP (strontium fluorovanadate) at 80 K (Peale et al. 1995).

## Results

The morphology of the as-grown undoped calcite crystals consists primarily of individual clear crystal rhombs with dimensions up to 3 mm. Some white spherical aggregates, consistent with previously reported vaterite morphology (Davies et al. 1978), were also identified. Nd<sup>3+</sup> doped crystals were slightly opaque and irregular, consisting of some large ~2000 μm aggregates of acicular crystals, some smaller ~100 μm multifaceted pieces, and other forms. No individual well-formed calcite rhombs were present in the doped material. However, characteristic 78° and 102° angles between facets were observed in some of the smaller crystals, which are consistent with the common (10 $\bar{1}$ 4) calcite form, corresponding to perfect cleavage.

Rutherford Backscattering

The RBS spectrum of Nd:CaCO<sub>3</sub> is shown in Figure 1 (dots). Nd, Ca, O, and C signals are labeled. The Nd signal is slightly peaked at high energy indicating a possibly higher Nd concentration on the surface layer (Czanderna and Hercules 1991). The line (Fig. 1) represents the simulated RBS spectrum created with RUMP (Doolittle 1985). Simulation parameters indicate a Nd concentration of  $0.05 \pm 0.01$  atomic % in the bulk of the Nd:CaCO<sub>3</sub> pellet, and twice that concentration at the surface.

### Energy-dispersive Spectrometry

The EDS fluorescence spectrum of Nd:CaCO<sub>3</sub> is shown in Figure 2. X-ray fluorescence peaks from the sample are present for Ca, C, O, and Nd. A weak Al peak appears as an artifact from the sample holder. The C peak may be slightly enhanced since the sample was mounted with conductive carbon tape. The small Cl peak may indicate the presence of some residue on the sample surface or a Cl impurity. However, a residue is unlikely since the samples were thoroughly rinsed with deionized water. The Nd concentration was determined from normalized k-ratios of Nd-L<sub>α</sub> and Ca-K<sub>α</sub> characteristic x-ray peak intensities using a standardless ZAF corrected (Scott and Love 1983) quantitative analysis. Concentration information from this spectrum was averaged with two others giving [Nd] =  $0.18 \pm 0.02$  atomic %.

### Powder X-ray Diffraction

Figure 3 shows the powder x-ray diffraction spectrum for (a) Nd doped samples and (b) undoped synthetic CaCO<sub>3</sub> crystals. These data have been normalized to the high intensity ( $10\bar{1}4$ ) reflection at 29.4° (Cu K<sub>α</sub> radiation) and scaled to reveal details of low

intensity data. The two spectra have almost identical features, which correlate with reference powder diffraction data (Swanson et al. 1953) for calcite (R -3 c) shown in Figure 3(c). There is no evidence of other  $\text{CaCO}_3$  phases in (a) or for residual  $\text{NdCl}_3$ . In the undoped sample, there are six small peaks  $\sim 85$  times smaller than the main calcite peak in Fig. 3(b) at  $21.1^\circ$ ,  $25.1^\circ$ ,  $27.2^\circ$ ,  $32.9^\circ$ ,  $43.9^\circ$ , and  $50.2^\circ$  (indicated by arrows). These peaks indicate traces of vaterite, a metastable polymorph of  $\text{CaCO}_3$ , whose reference powder diffraction spectrum (Rouse 1980) is shown in Figure 3(d). Spherical aggregates of vaterite were produced during the growth of undoped calcite, causing some phase contamination. Aragonite is another common, though metastable phase of  $\text{CaCO}_3$  that is known to form at room temperature and atmospheric pressure (Togari and Togari 1955), but there is no evidence of the aragonite phase in Fig. 3(a, b). Reference powder diffraction data (Keller et al. 1989) for aragonite (Pmcn) is shown in Figure 3(e).

#### Micro X-Ray Fluorescence

The ratio of Nd- $L_\alpha$  (5.230 keV) to Ca- $K_\alpha$  (3.691 keV) x-ray fluorescence is shown in the  $\mu\text{XRF}$  image in Figure 4(a), where lighter areas indicate higher ratio values. The calcite grain shown is approximately  $650\ \mu\text{m}$  across the bottom edge. The bright regions near step edges on the left and the dark region along the right of the sample are edge effects that can be understood as follows. Re-absorption by Ca, which decreases strongly with increasing photon energy, is the main cause of fluorescence attenuation within the crystal. Ca- $K_\alpha$  fluorescence is attenuated more since it has lower energy than Nd- $L_\alpha$  fluorescence, so higher ratios (Nd/Ca) are observed where the fluorescence path length within the crystal is longer. In Figure 4(a), exciting x-rays are incident from the left of

normal, allowing deep excitation near left facing step edges, which results in longer internal fluorescence path lengths and hence higher Nd/Ca ratio. On right-facing edges, since fluorescence is measured on the right of normal, fluorescence has a shorter path length through the sample, which enhances the relative Ca fluorescence yield and gives lower Nd/Ca values. The Nd/Ca ratio is fairly constant over the remaining area of the crystal surface.

### XAFS Spectroscopy

Figure 5 shows a comparison of the  $k^3$ -weighted XAFS spectra of Nd:CaCO<sub>3</sub> (light) and Nd<sub>2</sub>(CO<sub>3</sub>)<sub>3</sub>·xH<sub>2</sub>O (heavy) after background subtraction, normalization, and conversion to k-space. Nd<sub>2</sub>(CO<sub>3</sub>)<sub>3</sub>·xH<sub>2</sub>O has slightly higher frequency oscillations corresponding to a larger first shell radius.

The heavy line in Figure 6 is the Fourier transform magnitude of the  $k^3$ -weighted data from Figure 5 for the Nd:CaCO<sub>3</sub> sample. The small peak at low R is an artifact from background subtraction. The dotted line in Figure 6 shows the best fit using four scattering shells and assuming that Nd<sup>3+</sup> occupies the Ca<sup>2+</sup> site in calcite. Single scattering events from the first (Nd-O<sub>1</sub>), second (Nd-C), third (Nd-O<sub>2</sub>), and fourth (Nd-Ca) atomic shells were considered. The data and corresponding fit give an average first shell (Nd-O<sub>1</sub>) radius of  $2.45 \pm 0.02 \text{ \AA}$  and a coordination number of  $10.3 \pm 1$  with Debye-Waller factor  $\sigma^2 = 0.014 \pm 0.002 \text{ \AA}^2$ . Higher order scattering shells were assigned a six-fold coordination corresponding to the ideal calcite structure. Fitting results indicate a second shell (Nd-C) radius of  $3.40 \pm 0.02 \text{ \AA}$  with  $\sigma^2 = 0.001 \pm 0.002 \text{ \AA}^2$ , third shell (Nd-O<sub>2</sub>) radius  $3.57 \pm 0.03 \text{ \AA}$  with  $\sigma^2 = 0.001 \pm 0.002 \text{ \AA}^2$ , and fourth shell (Nd-Ca) radius  $3.95$

$\pm 0.03 \text{ \AA}$  with  $\sigma^2 = 0.034 \pm 0.002 \text{ \AA}^2$ . The corresponding scattering shell radii in an ideal calcite structure are  $2.36 \text{ \AA}$  (Ca-O<sub>1</sub>),  $3.21 \text{ \AA}$  (Ca-C),  $3.46 \text{ \AA}$  (Ca-O<sub>2</sub>), and  $4.04 \text{ \AA}$  (Ca-Ca), indicating substantial lattice dilation around the Nd<sup>3+</sup> impurity.

### Near Infrared Absorption

Figure 7 shows the  $^4I_{9/2} \rightarrow ^4F_{3/2}$  absorption band for Nd:CaCO<sub>3</sub> at 300 K, 90 K, and 8 K. There is some line sharpening as the sample is cooled from 300 K to 90 K, but no further change is observed in the spectra as it is cooled to 8 K. The  $^4G_{5/2} + ^2G_{7/2}$  and  $^2K_{13/2} + ^4G_{7/2}$  absorption bands were also observed in the upper visible, and the  $^4I_{13/2}$  and  $^4I_{15/2}$  bands were observed in the mid IR with only moderate interference from calcite lattice bands. Lattice bands obscured the  $^4I_{11/2}$  band. In all bands, the same temperature dependence was observed.

Absorption spectra of model compounds were measured to test the question whether the observed absorption lines arise from Nd<sup>3+</sup> actually in calcite or from a second phase, such as Nd<sub>2</sub>(CO<sub>3</sub>)<sub>3</sub>, or as a residue of NdCl<sub>3</sub> on the crystal surface (though not detected in powder XRD, Fig. 3(a)). Figure 8 compares the 8 Kelvin NdCl<sub>3</sub>·6H<sub>2</sub>O, Nd<sub>2</sub>(CO<sub>3</sub>)<sub>3</sub>, and Nd:CaCO<sub>3</sub> pressed pellet spectra, which are seen to differ substantially in width, position, and number of lines. The  $^4F_{5/2} + ^2H_{9/2}$  and  $^4F_{7/2} + ^4S_{3/2}$  bands were also observed to differ markedly for the two samples.

### Micro Photoluminescence

Though pellet absorption spectra of Nd:CaCO<sub>3</sub> and Nd<sub>2</sub>(CO<sub>3</sub>)<sub>3</sub>·xH<sub>2</sub>O differ, they are similar enough to motivate additional comparison. Nd<sup>3+</sup> fluorescence was measured with

a micro Raman spectroscopy setup in order to allow measurement of low fluorescence yields from individual as-grown crystal grains. This reduces the averaging over grains that occurs in pellet spectra. Figure 9(a) shows the  $\text{Nd}^{3+} \ ^4\text{F}_{3/2} \rightarrow \ ^4\text{I}_{9/2}$  transitions from a Nd:CaCO<sub>3</sub> crystal aggregate (~1200 μm) at 90 K. This spectrum is typical of all samples measured, aside from differences in noise level and counting rate, which were correlated to the grain size. The smallest sample measured successfully was a single ~400 μm grain. The line shape appears to be independent of the number of grains excited. Figure 9(b) shows the same  $\text{Nd}^{3+}$  transition in Nd<sub>2</sub>(CO<sub>3</sub>)<sub>3</sub>·xH<sub>2</sub>O. The spectral differences in the number of lines and line widths between these two samples are even stronger than in the absorption data.

### Mid-IR Spectroscopy

A comparison of mid-IR absorption spectra for a natural calcite sample (light) and an undoped solution grown calcite rhomb (heavy) is shown in Figure 10. The usual calcite lattice bands have nearly equal strength for the two samples. The synthetic crystal has a strong water absorption band centered at 3300 cm<sup>-1</sup> (Robinson 1974). This band is absent (or much weaker) in the natural calcite spectrum.

### Discussion

A Nd concentration of  $0.05 \pm 0.01$  atomic % was determined by RBS analysis of doped synthetic calcite. The RBS value is favored over the EDS value of 0.18 atomic % because several potential sources of error exist for EDS. EDS was performed on as-grown calcite particles that differed in size and orientation, and irregular surface

topography alters x-ray absorption characteristics (Scott and Love 1983). Also, subtle variations in subtraction of the x-ray fluorescence background could dramatically alter the resulting Nd concentration.

Calcite phase purity was verified by powder x-ray diffraction, and the sharp x-ray lines show that it is well crystallized. However, a second Nd-containing phase might go undetected if present below 1 %. Mapping by  $\mu$ XRF indicates a fairly uniform distribution of  $\text{Nd}^{3+}$  ions in the as-grown crystal grains, which would seem unlikely if the Nd were concentrated in a second phase. A Nd XAFS comparison of our samples with standard  $\text{Nd}_2(\text{CO}_3)_3 \cdot x\text{H}_2\text{O}$  reveals differences in structure, and there are clear differences in the number of lines, line width, and center frequency in near-IR absorption and fluorescence spectra between Nd: $\text{CaCO}_3$  samples and  $\text{Nd}_2(\text{CO}_3)_3 \cdot x\text{H}_2\text{O}$  or  $\text{NdCl}_3 \cdot 6\text{H}_2\text{O}$  standards. Hence both XAFS and optical measurements support the conclusion that  $\text{Nd}^{3+}$  signals in our samples originate from  $\text{Nd}^{3+}$  in calcite, not other crystalline phases.

XAFS analysis of Nd: $\text{CaCO}_3$  shows that the local lattice distortion is substantial. XAFS supports the conclusion that Nd is substitutional for Ca in calcite, but with an increase in first shell (Nd-O) radius and coordination, as well as some lattice dilation in the second and third coordination shells. Other studies of lanthanide impurities in calcite are consistent with this result, reporting 6-fold coordination for the smaller lanthanides Dy and Yb and 7-fold coordination for the larger lanthanides Nd and Sm (Elzinga et al. in press). Possible mechanisms whereby an additional oxygen atom is incorporated within the first coordination shell have been proposed (Elzinga et al. in press). The same effect is absent in smaller trivalent REEs, suggesting a disparity in the charge compensation mechanism across the lanthanide series.

The large line width and absence of line sharpening below 90 K for the near-IR absorption spectra indicate a high degree of inhomogeneous broadening. In other charge compensated Nd-doped crystals, such as melt-grown Nd:Strontium fluoroapatite (Fig. 11) (Peale et al. 1995), where different crystal-field environments give rise to discrete lines that can be more or less resolved, line widths at 300 K are tens of  $\text{cm}^{-1}$ , decrease to a few  $\text{cm}^{-1}$  at liquid nitrogen temperature, and can decrease further even to sub- $\text{cm}^{-1}$  widths at liquid helium temperature (Hong et al. 1995). Discrete lattice effects dominate the Nd:SVAP spectrum (Fig. 11) with only a weak continuous background. In contrast, although the usual two  ${}^4\text{F}_{3/2}$  lines are seen in Fig. 7, each has a temperature independent width of  $\sim 80 \text{ cm}^{-1}$  below 90 K. Because the lines are smooth, without discrete structure, one may infer that the very large widths result from a broad and continuous distribution of crystal field environments. As Figure 11 shows, a distribution of discrete center frequencies, spanning several hundred  $\text{cm}^{-1}$  in charge compensated  $\text{Nd}^{3+}$  doped crystals, is not unusual, but the smoothness of this distribution in calcite is more characteristic of glassy (Mann and DeShazer 1970) than crystalline hosts. Yet the powder x-ray diffraction shows that our samples are well crystallized. The apparent independence on sample size of the micro photoluminescence line shapes show that the broad line widths come from a distribution within individual grains and not among grains.

Dieke (1968) reports that broad absorption lines, such as those for Nd: $\text{CaCO}_3$ , have been observed repeatedly from rare earth ions in solution grown crystals, and he attributes the broadening to non-uniform lattice strain. Lattice strain induced by water inclusions may contribute to the broadening of  $\text{Nd}^{3+}$  lines. The presence of water is supported by mid-IR spectra (Fig. 10), which reveal strong water-related absorption bands

in solution-grown crystals that are absent in natural calcite samples. Broad  $\text{Nd}^{3+}$  absorption lines are also observed in the absorption spectra of the two reference compounds (Fig. 9(a))  $\text{NdCl}_3 \cdot 6\text{H}_2\text{O}$  and  $\text{Nd}_2(\text{CO}_3)_3 \cdot x\text{H}_2\text{O}$  with approximate linewidths at 8 K of  $25 \text{ cm}^{-1}$  and  $40 \text{ cm}^{-1}$  respectively, while  $\text{Nd}:\text{CaCO}_3$  has linewidths of  $80 \text{ cm}^{-1}$ . Since these two hydrophilic reference compounds are likely hydrated to a higher degree than  $\text{Nd}:\text{CaCO}_3$ , yet their line widths are less, the high degree of broadening observed in our samples is difficult to explain by hydration-induced lattice strain alone.

Hydroxylation of  $\text{Nd}^{3+}$  in the  $\text{Ca}^{2+}$  site is a possibility. The extra oxygen in the first shell of  $\text{Nd}^{3+}$  (needed to explain the lattice distortion found by XAFS) could as well arise from a near neighbor hydroxyl ion impurity as from bidentate linkage of a carbonate group. Such an  $\text{OH}^-$  ion would effect the necessary charge compensation.

Implications may be drawn from this study of  $\text{Nd}:\text{CaCO}_3$  regarding long-term retention or remobilization of  $\text{Nd}^{3+}$ -like ions from calcite minerals. The incorporation of Nd in calcite with substantial lattice dilation indicates large local strain. This implies an increase in Gibbs free energy and higher dissolution rate. This assertion is supported by simulations of crystal dissolution (Lasaga et al. 2001) which show that defect centers act as dissolution nucleation sites on mineral surfaces. At high undersaturation conditions, these nucleation sites develop into etch pits with emanating dissolution stepwaves that extend over the crystal surface causing global dissolution (Lasaga et al. 2001).

We end this paper by making some testable hypotheses. The strain field associated with  $\text{Nd}^{3+}$  ions in calcite should cause etch pit formation and increase the overall mineral dissolution rate. The actinide elements  $\text{Pu}^{3+}$ ,  $\text{Am}^{3+}$  and  $\text{Cm}^{3+}$  are likely to exhibit similar behavior since they have the same valence and similar ionic radii as  $\text{Nd}^{3+}$ .

The Nd<sup>3+</sup>-like REEs are more likely to remobilize than REEs with higher site compliance in calcite minerals.

### **Acknowledgments**

This research was supported by DOE grant DE-FG07-99ER15013 through the Environmental Management Science Program, and an AWU fellowship. The authors wish to express their gratitude to B. P. Tonner, B. H. T. Chai, and E.J. Elzinga for their useful suggestions, to S. Heald, and R. Gordon for assistance with XAFS data collection at the APS, and to C. Rivero for assistance with fluorescence measurements.

## References

- Anderson FG, Summers PL, Weidner H, Hong P, Peale RE (1994) Interpretive crystal field parameters: Application to  $\text{Nd}^{3+}$  in  $\text{GdVO}_4$  and  $\text{YVO}_4$ . *Phys Rev B* 50: 14802
- Bünzli J-CG, Choppin GR (eds) (1989) *Lanthanide Probes in Life, Chemical and Earth Sciences*, Elsevier Science Publishers, New York.
- Czanderna AW, Hercules DM (eds) (1991) *Ion Spectroscopies for Surface Analysis*, New York : Plenum Press.
- Davies P, Dollimore D, Heal GR (1978) Polymorph transition kinetics by DTA. *J Therm Anal* 13(3): 473-487
- Dieke GH (1968) *Spectra and energy levels of rare earth ions in crystals*, John Wiley & Sons, New York.
- Doolittle LR (1985) Algorithms for the rapid simulation of rutherford backscattering spectra. *Nucl Instrum Meth B* 9(3): 344-351
- Effenberger H, Mereiter K, Zemann J (1981) Crystal-structure refinements of magnesite, calcite, rhodochrosite, siderite, smithonite, and dolomite, with discussion of some aspects of the stereochemistry of calcite type carbonates. *Z Kristallogr* 156(3-4): 233-243
- Elzinga EJ, Reeder RJ, Withers SH, Peale RE, Mason RA, Beck KM, Hess WP (in press) XAFS Study of Rare Earth Element Coordination in Calcite. *Geochim Cosmochim Acta*
- Gruzensky PM (1967) Proceedings of the International Conference on Crystal Growth (Boston, 20-24 June 1966), Peiser HS (ed), Pergamon, New York, pp 365-367
- Hong P, Zhang XX, Peale RE, Weidner H, Bass M, Chai BHT (1995) Spectroscopic characteristics of  $\text{Nd}^{3+}$ -doped strontium fluorovanadate and their relationship to laser performance. *J Appl Phys* 77(1): 294-300
- JADE for Windows V3.1 XRD Pattern Processing for the PC (1995) [Computer Software]. Materials Data, Inc.
- Keller L, Rask J, Buseck P (1989) Arizona State Univ., Tempe, AZ, USA, PDF#41-1475. Retrieved from JADE for Windows V3.1 Powder Diffraction File.
- Lasaga AC, Luttge A (2001) Variation of Crystal Dissolution Rate Based on a Stepwave Model. *Science* 291: 2400
- Mann MM and DeShazer LG (1970) Energy Levels and Spectral Broadening of Neodymium Ion in Laser Glass. *J. Appl. Phys.* 41:2951-2957

Mecherri OM, Budiman-Sastrowardoyo P, Rouchaud JC, Fedoroff M (1990) Study of Neodymium Sorption on Orthose and Calcite for Radionuclide Migration Modelling in Groundwater. *Radiochim Acta* 50: 169-175

Peale RE, Summers PL, Weidner H, Chai BHT, Morrison CA (1995) Site-selective spectroscopy and crystal-field analysis for Nd<sup>3+</sup> in strontium fluorovanadate. *J Appl Phys* 77(1): 270-276

Reeder RJ, Lambie GM, Northrup PA (1999) XAFS study of the coordination and local relaxation around Co<sup>2+</sup>, Zn<sup>2+</sup>, Pb<sup>2+</sup>, and Ba<sup>2+</sup> trace elements. *Am Mineral* 84(7-8): 1049-1060

Reeder RJ, Nugent M, Lambie GM, Tait CD, Morris DE (2000) Uranyl incorporation into calcite and aragonite: XAFS and luminescence studies. *Environ Sci Technol* 34(4): 638-644

Rehr JJ, Zabinsky SI, Albers RC (1992) High-Order Multiple-Scattering Calculations of X-Ray-Absorption Fine-Structure. *Phys Rev Lett* 69(23): 3397-3400

Ressler T (1997) WinXAS: A new software package not only for the analysis of energy-dispersive XAS data. *J Phys IV* 7(C2): 269-270

Robinson JW (ed) (1974) *Handbook of Spectroscopy v II*, CRC Press, Cleveland, p 78

Rouse R (1980), Dept. of Geological Sciences, Univ. of Michigan, Ann Arbor, MI, USA, PDF#33-0268. Retrieved from JADE for Windows V3.1 Powder Diffraction File.

Scott VD, Love G (1983) *Quantitative Electron-Probe Microanalysis*, John Wiley & Sons, New York.

Shannon RD (1976) Revised effective ionic-radii and systematic studies of interatomic distances in halides and chalcogenides. *Acta Crystallogr A* 32: 751-767

Slate JL (1996) Buried carbonate paleosols developed in Pliocene-Pleistocene deposits of the Pasco Basin, south-central Washington, U.S.A. *Quaternary International*, 34-36, 191-196.

Swanson HE, Fuyat RK, Tatge E (1953) *Natl. Bur. Stand. (US), Circ. 539, II 51*, PDF#05-0586. Retrieved from JADE for Windows V3.1 Powder Diffraction File.

Togari K, Togari S (1955) *Journ Fac Sci* 9: 55

Zhong S, Mucci A (1995) Partitioning of rare earth elements (REEs) between calcite and seawater solutions at 25°C and 1 atm, and high dissolved REE concentrations. *Geochim Cosmochim Acta* 59: 443-453

## Figure Legends

Figure 1. Raw RBS spectrum (dots) and fitted spectrum (line) of  $\text{Nd}^{3+}:\text{CaCO}_3$ .

Figure 2. EDS spectrum of  $\text{Nd}^{3+}:\text{CaCO}_3$

Figure 3. The normalized powder x-ray diffraction spectra of (a) synthetic  $\text{Nd}:\text{CaCO}_3$ , (b) synthetic undoped  $\text{CaCO}_3$ , (c) reference data for calcite (Swanson and Tatge 1953), (d) reference data for vaterite (Rouse 1980), and (e) reference data for aragonite (Keller et al. 1989).

Figure 4. (a)  $\mu\text{XRF}$  map of the  $\text{Nd}/\text{Ca}$  fluorescence ratio from a single polished calcite grain. Lighter areas indicate higher  $\text{Nd}$  concentration. The image is  $750\ \mu\text{m}$  wide and  $850\ \mu\text{m}$  high. (b) An intensity profile corresponding to the slice indicated in (a).

Figure 5.  $k^3$ -weighted  $\chi(k)$  spectra for  $\text{Nd}^{3+}:\text{CaCO}_3$  (light) and  $\text{Nd}_2(\text{CO}_3)_3 \cdot x\text{H}_2\text{O}$  (heavy).

Figure 6. The Fourier transform magnitude of the  $k^3$ -weighted experimental (solid) XAFS spectrum of  $\text{Nd}^{3+}:\text{CaCO}_3$  and a calculated fit (dotted) for  $\text{Nd}^{3+}$  in calcite.

Figure 7. Near-IR pellet absorption spectra of  $^4\text{I}_{9/2} \rightarrow ^4\text{F}_{3/2}$  transitions in  $\text{Nd}:\text{CaCO}_3$  at 300 K, 90 K, and 8 K.

Figure 8. Near-IR pellet absorption spectra of  $\text{Nd}^{3+}$  in (a)  $\text{Nd}:\text{CaCO}_3$ ,  $\text{Nd}_2(\text{CO}_3)_3 \cdot x\text{H}_2\text{O}$  and  $\text{NdCl}_3 \cdot 6\text{H}_2\text{O}$  at 8 K.

Figure 9. Near-IR fluorescence spectra of  $^4\text{F}_{3/2} \rightarrow ^4\text{I}_{9/2}$  transitions at 90 K in  $\text{Nd}:\text{CaCO}_3$  and  $\text{Nd}_2(\text{CO}_3)_3 \cdot x\text{H}_2\text{O}$ .

Figure 10. Mid-IR transmittance spectra of synthetic (heavy) and natural (light) calcite samples.

Figure 11.  $^4\text{I}_{9/2} \rightarrow ^4\text{F}_{3/2}$  absorption spectrum of  $\text{Nd}:\text{SVAP}$  at 2 K from (Peale et al. 1995).

Figure 1.  
Withers et al.  
Phys Chem Minerals

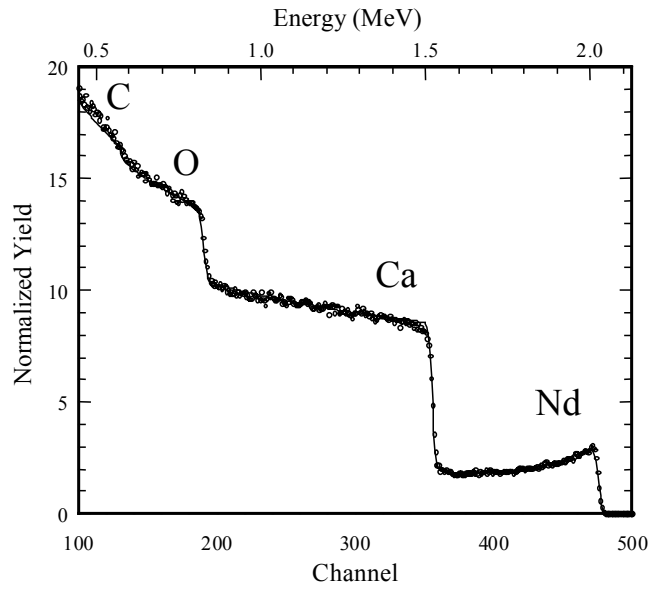


Figure 2.  
Withers et al.  
Phys Chem Minerals

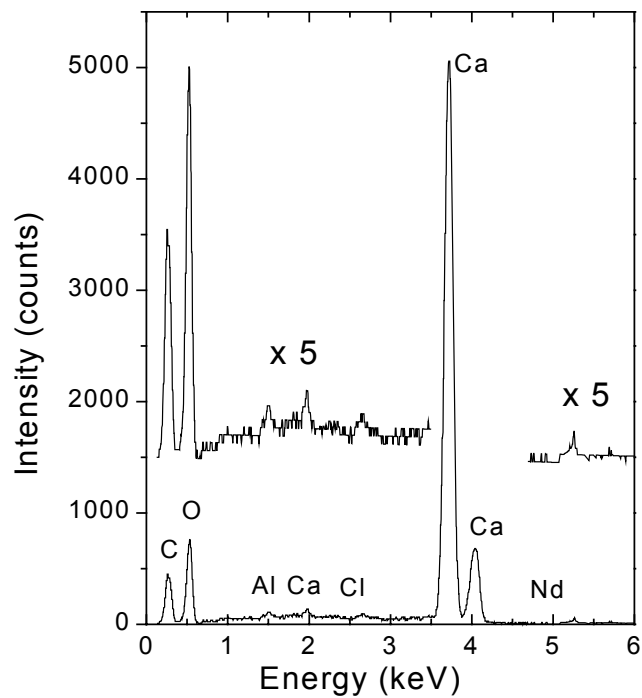


Figure 3.  
Withers et al.  
Phys Chem Minerals

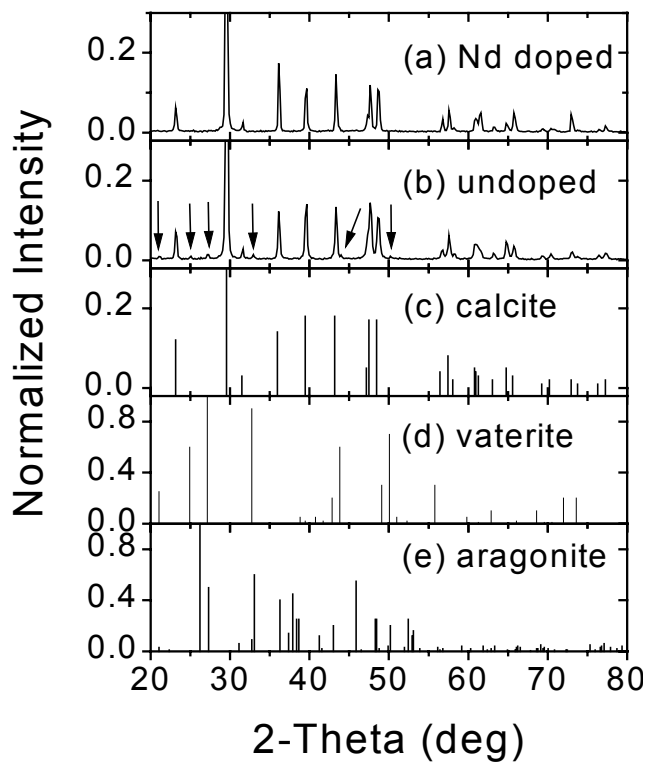


Figure 4.  
Withers et al.  
Phys Chem Minerals

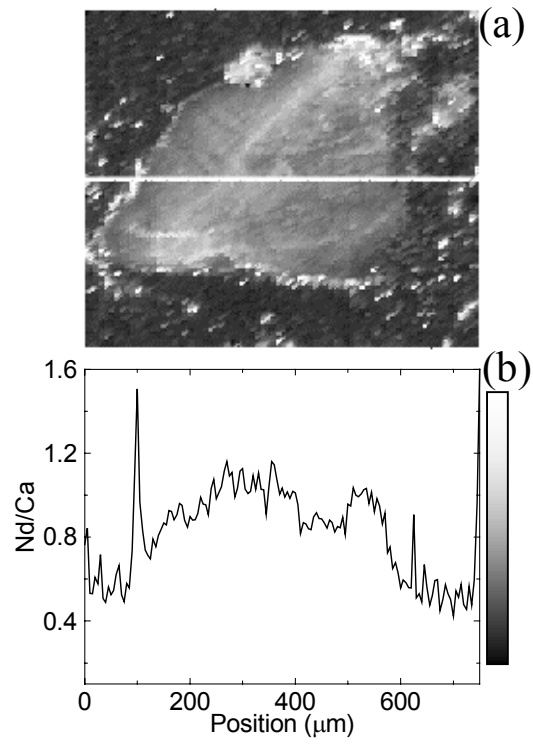


Figure 5.  
Withers et al.  
Phys Chem Minerals

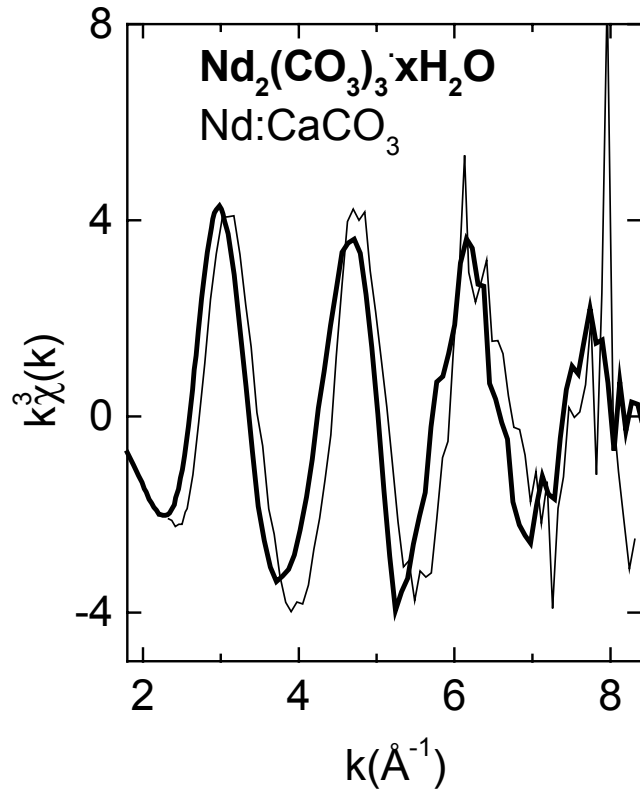


Figure 6.  
Withers et al.  
Phys Chem Minerals

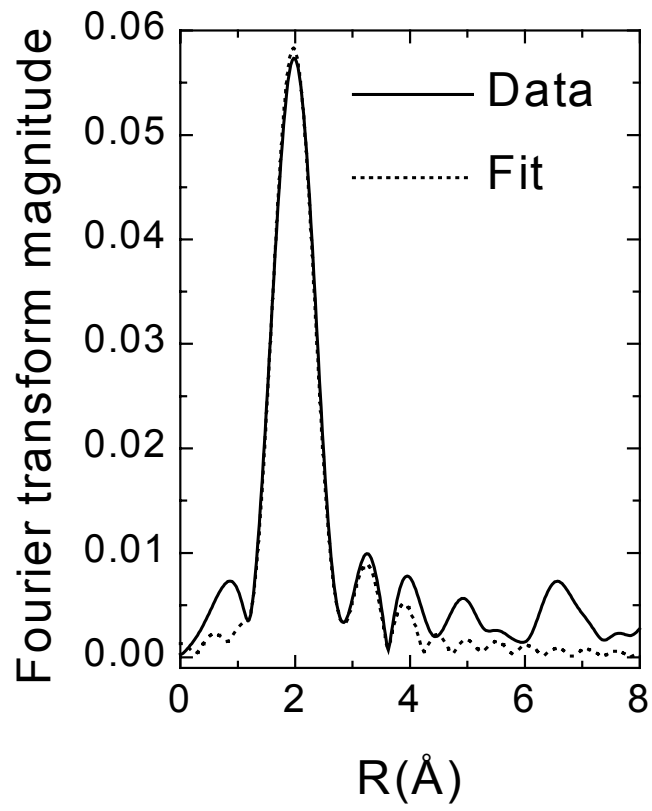


Figure 7.  
Withers et al.  
Phys Chem Minerals

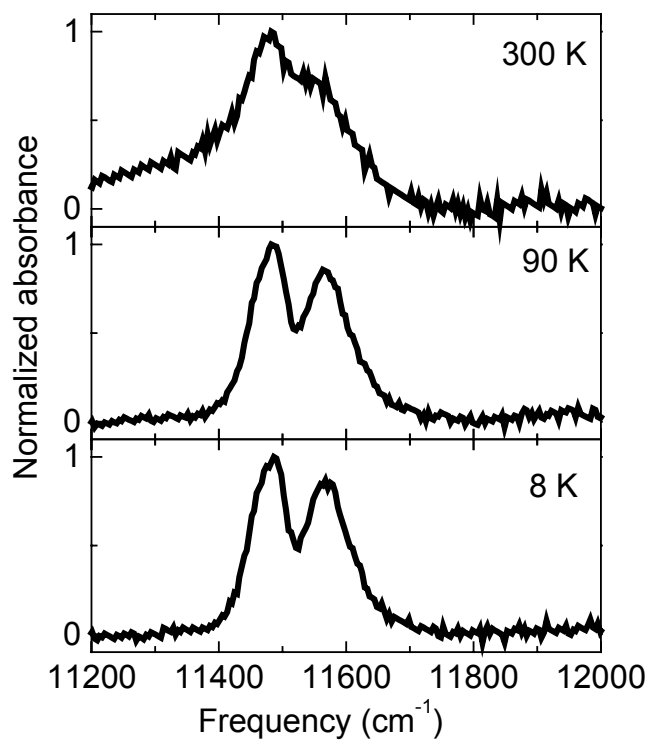


Figure 8.  
Withers et al.  
Phys Chem Minerals

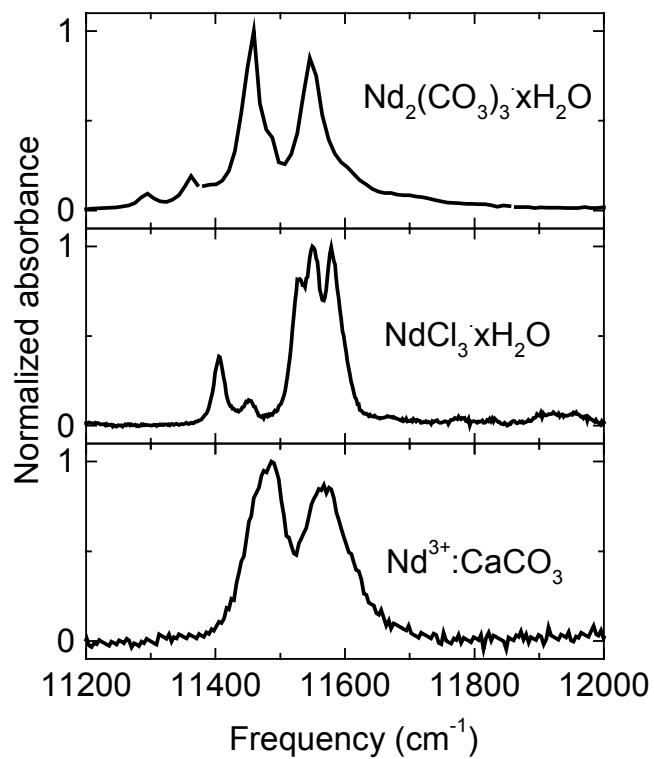


Figure 9.  
Withers et al.  
Phys Chem Minerals

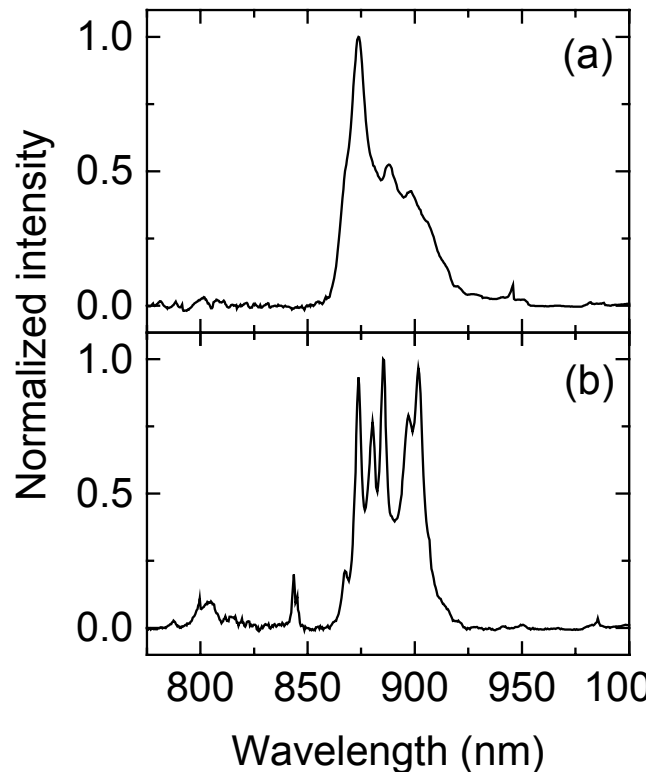


Figure 10.  
Withers et al.  
Phys Chem Minerals

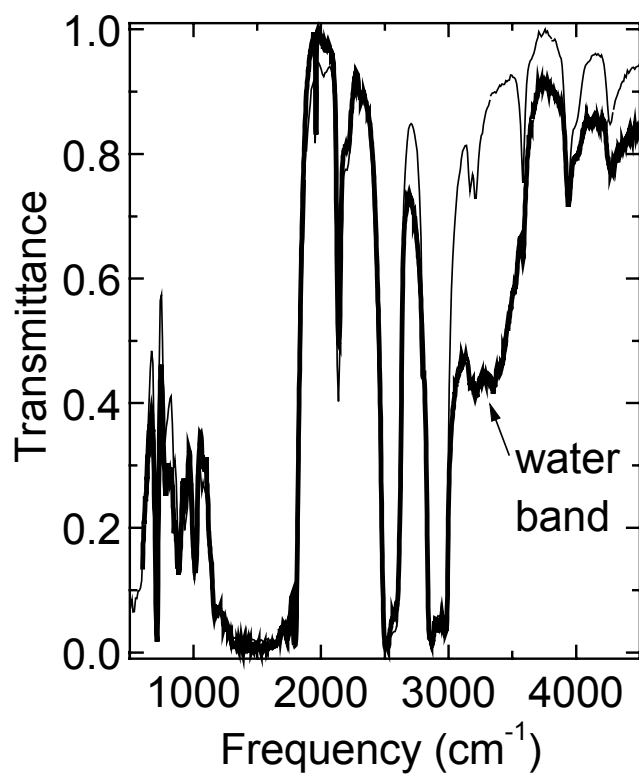


Figure 11.  
Withers et al.  
Phys Chem Minerals

